纳米 Cu_2O/珍珠贝壳复合光催化材料的制备及其在有机染料处理中的应用

邹晓兰[1,2], 于艳卿[1,2], 李超峰[1,2], 朱校斌[1,*]

[1]中国科学院海洋研究所, 山东青岛 266071

[2]中国科学院研究生院, 北京 100049

摘要: 将珍珠贝壳废弃物活化并作为载体, 应用原位水解法制备出 Cu_2O/珍珠贝壳复合材料. 运用 X 射线衍射、X 射线光电子能谱、扫描电镜、紫外-可见漫反射吸收光谱对复合材料进行表征. 用活性大红染料 B-3G 水溶液作为模拟废水评价复合材料在可见光下的催化性能. 结果表明, 负载的 Cu_2O 呈椭球形, 理论平均粒径为 16.8 nm. 复合材料对紫外和可见光谱均有吸收. 相对纯 Cu_2O 而言, 纳米 Cu_2O/珍珠贝壳复合材料在催化有机染料降解脱色实验中具有更高的活性, 在适宜的环境条件下 (pH 为 6.0~12.0, 反应时间为 90 min, B-3G 初始浓度 ≤ 220 mg/L), 催化 B-3G 降解脱色率达 98%, 催化反应过程符合伪一级反应动力学模型. 此外, 傅里叶变换红外光谱研究表明, 纳米 Cu_2O/珍珠贝壳复合材料的形成源于 Cu_2O 和 CaO 间的结合并发生相互作用.

关键词: 珍珠贝壳; 原位水解; 纳米 Cu_2O; 光催化; 染料 B-3G

中图分类号: O643　　　**文献标识码**: A

Preparation of Nano-Cu_2O/Pearl Shell Composites for Treating Organic Dyes

ZOU Xiaolan[1,2], YU Yanqing[1,2], LI Chaofeng[1,2], ZHU Xiaobin[1,*]

[1]*Institute of Oceanology, Chinese Academy of Sciences, Qingdao 266071, Shandong, China*

[2]*Graduate University of Chinese Academy of Sciences, Beijing 100049, China*

Abstract: Waste pearl shells were activated and used as carriers to prepare a nano-Cu_2O/pearl shell composite photocatalyst by in situ hydrolysis. The composites were characterized by X-ray diffraction, X-ray photoelectron spectrometer, scanning electron microscopy, and UV-Vis diffuse reflectance spectrometer. Reactive red dye B-3G solutions were used as simulate wastewater to investigate the photocatalytic performance under visible light irradiation. The loaded Cu_2O particles had an average diameter of 16.8 nm, were oval in shape and have absorption bands in the UV and visible region similar to those of pure Cu_2O particles. The nano-Cu_2O/pearl shell composites had much higher photocatalytic activities than pure Cu_2O. Over 98% of the B-3G solutes were decolorized by these composites under the conditions of pH = 6.0–12.0, reaction time = 90 min, and B-3G concentration ≤ 220 mg/L. The photocatalytic decolorization of B-3G followed pseudo-first order kinetics. The formation mechanism of the nano-Cu_2O/pearl shell composites was studied by Fourier transform infrared spectroscopy. It involved the interaction and combination of Cu_2O and CaO.

Key words: pearl shells; in situ hydrolysis; nano-Cu_2O; photocatalysis, dye B-3G

Large volumes of mollusk shells are discharged from many shellfish farms and marine product manufacturing plants. Untreated shell wastes have a nasty smell, and are mostly dumped and treated in landfills [1,2]. To reduce the quantity thrown away and increase the value of shell wastes, studies have been conducted to develop shell wastes as ingredients for construction materials [3], adsorbents for phosphates [1,4,5] and metal ions [6] in aqueous solutions, and additives to reinforce the mechanical strength of epoxy resin [7]. Millions of tons of pearl shell wastes from the pearl industry are discarded annually in China [7]. Pearl shells are hybrid composites of organic (matrix of proteins and chitins) and inorganic matter in the form of organic-inorganic interfaces [8,9], and are primarily composed of aragonite, which in turn consists of calcium carbonate.

Photocatalysis has been widely investigated for treating non-biodegradable organic pollutants. Nano-cuprous oxide (nano-Cu_2O), a typical metal oxide p-type semiconductor has attract much attention for its relatively small band gap between 2.0 and 2.2 eV, which makes it a promising visible light ($\lambda \leq 600$ nm) photocatalyst [10]. As compared with the traditional nano-TiO_2 photocatalyst whose utilization rate of the solar spectrum is only 3%–5% [11], nano-Cu_2O is a promising alternative for its increased utilization rate of the solar spectrum. However, nano-Cu_2O particles tend to aggregate in aqueous solutions, which decreases both surface area and photocatalytic efficiency [12]. Researchers have worked on stabilizing nano-Cu_2O particles on various carriers [12–18]. However, the use of hazardous chemical agents is unavoidable in the normal methods of stabilization, such as Cu^{2+} reduction [12,14,15], chemical vapor deposition [18], and polyol process [14,17].

In this study, we loaded nano-Cu_2O onto the surface of activated pearl shells by in situ hydrolysis without the use of toxic chemical agents. The physical properties of the nano-Cu_2O/pearl shell composites were characterized, and photocatalytic activities under visible light irradiation were evaluated by the decolorization of the reactive red dye B-3G. The kinetics of photocatalytic reaction and formation mechanism of the composites were obtained. This provides shell wastes a high value-added use and has the significance of using sunlight in the degrading of non-biodegradable organic water pollutants.

1 Experimental

1.1 Materials

The pearl shell wastes used in this work were supplied by Guangdong Anhua Group Co., Ltd. (Zhanjiang). NaCl was purchased from Tianjin Basifu Chemical Ltd. CuCl and sodium dodecyl benzene sulfonate (SDBS) were obtained from Tianjin Guangfu Fine Chemical Research Institute. All the reagents are analytical grade.

1.2 Preparation of the photocatalyst

1.2.1 Pretreatment of the pearl shell wastes

Collected pearl shell wastes were submerged in hydrochloric acid (0.1%) for 0.5 h to remove surface organic matter and impurities. Subsequently, these shells were washed and dried, calcined at 1050 °C for 2 h in a muffle furnace, ground, and sieved through a 100 mesh filter.

1.2.2 Preparation of Cu_2O/pearl shell composites

The Cu_2O/pearl shell composites were synthesized by in situ hydrolysis. CuCl (1.0 g) was added into a 100 ml thermodynamically stable micro-reaction system (aqueous solution containing NaCl and SDBS) with vigorous magnetic stirring. Then, 1.0 g of pretreated pearl shell powder was added into the mixture to hydrolyze CuCl into Cu_2O on the surface. Yellow precipitates (Cu_2O/pearl shell composites) were produced after stirring for 0.5 h. The precipitates were then cleaned by ultrasonic treatment for 2 min and washed five times with doubly distilled water to remove remaining SDBS and Cl⁻. The products were filtrated and dried at 60 °C for 6 h.

1.3 Characterization of Cu_2O/pearl shell composites

The crystalline phases of the composites were characterized by a Bruker D8 Advance X-ray diffraction spectrometer (XRD, Germany) using Cu K_α radiation ($\lambda = 0.15406$ nm). The X-ray photoelectron spectra (XPS) were obtained by a PHI-5000C ESCA system XPS spectrometer (USA) with Al K_α radiation ($h\nu = 1486.6$ eV). Microstructures and morphologies were investigated using a JSM-6700F scanning electron microscope (SEM, Japan). Diffuse reflection spectra were obtained using a Cary 5000 UV-vis spectrometer (USA). Fourier transform infrared (FT-IR) spectra were obtained with a Nicolet iS10 FT-IR spectrometer (USA) to study the formation mechanism. The mean diameter of the Cu_2O nanoparticles was calculated by the Scherrer Equation, Eq. (1), with the full width of the half maximum of the diffraction peak (FWHM) at 2θ in the XRD pattern:

$$L = k\lambda/\beta\cos\theta \qquad (1)$$

where L is the mean diameter of the particles, β is FWHM, θ is the diffraction angle, λ is the wavelength of Cu K_α radiation ($\lambda = 0.15406$ nm), and k is a constant equal to 0.89.

1.4 Photocatalytic reaction

Reactive red dye B-3G solutions were used as a model organic waste water to investigate the photocatalytic activity. The catalyst (30 mg) was added to 15 ml B-3G aqueous solution. An air pump was used to stir the liquid and supply oxygen. The visible light source was a Philips Iodine–Tungsten lamp (500 W; wavelength range = 400–800 nm [16]) fitted in a quartz cold trap. The average light intensity used was 127300 lux. B-3G water samples were centrifuged to separate catalyst particles from the solutions. The filtrate was analyzed by a PGENERAL T6 UV-vis spectrophotometer (China) at λ_{max}= 509 nm. The decolorization efficiency of B-3G was calculated from the initial and final absorbance of the B-3G solutions using

$$\text{Decolorization (\%)} = (A_0 - A_t)/A_0 \times 100\% \qquad (2)$$

where A_0 is the initial absorbance of B-3G and A_t is the absorbance of B-3G after t minutes of reaction.

The kinetics of the photocatalytic reactions under visible light of the photocatalytic decolorization of B-3G were studied with 2 g/L nano-Cu_2O/pearl shell composites added into the B-3G solutions. The photocatalytic reaction was described as pseudo-first order by Eq. 3:

$$-dc/dt = kc \qquad (3)$$

where k is the pseudo-first order rate constant. Eqs. 4 and 5 were used with the concentration $c = c_0$ at reaction time $t = 0$:

$$c = c_0 e^{-kt} \qquad (4)$$

$$\ln(c_0/c) = kt \qquad (5)$$

The half-times ($t_{1/2}$) were obtained as

$$t_{1/2} = \ln(2/k) \qquad (6)$$

2 Results and Discussion

2.1 Characterization of the Cu_2O/pearl shell composite photocatalysts

Figure 1 shows the SEM images of the activated pearl shells and Cu_2O/pearl shell composites synthesized by in situ hydrolysis. Fig. 1 (a) shows that the morphology of the shells became loose and porous after 2 h of activation at 1050 °C. All organic materials were totally decomposed and CO_2 was released from $CaCO_3$. The shell surfaces had uniform micron-sized pores with bending channels, which provided space and sites for Cu_2O to be loaded onto. The direct evidence of Cu_2O particle formation on the surface of the pearl shells is shown in Fig. 1 (b) and (c). The loaded Cu_2O particles appeared oval in shape, and were well dispersed in the micron-sized channels of the pearl shells, leading to the generation of smaller hole channels. The sizes of the Cu_2O particles were not larger than 100 nm. There was a strong interaction between the Cu_2O nanoparticles and pearl shells due to the hydrolysis sites provided by the large pores and high alkalinity of the pearl shells. Nano-Cu_2O/pearl shell composites were successfully synthesized. The energy dispersion spectroscopy (EDS) spectra proved the absence of unwanted impurities in both the pearl shells and nano-Cu_2O/pearl shell composites.
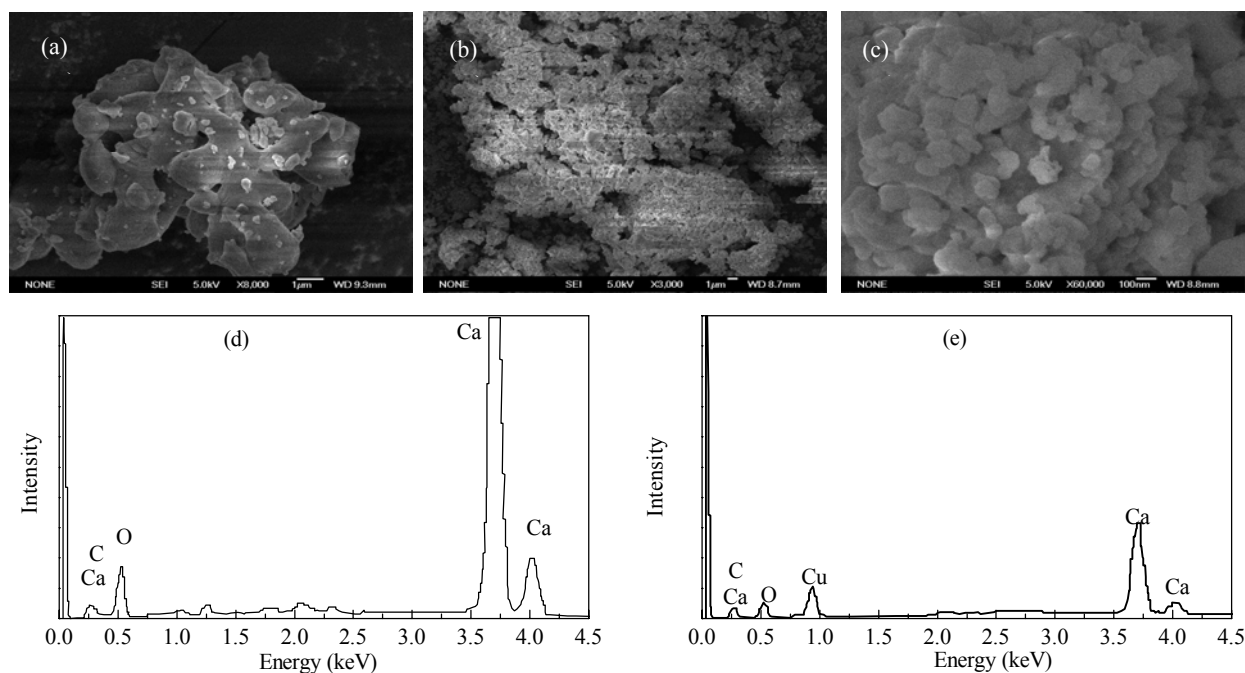
Fig. 1. SEM images of pearl shells calcined at 1050 °C (a), Cu_2O/pearl shell composites at low magnification (b), and Cu_2O/pearl shell composites at high magnification (c) and EDS spectra of pearl shells calcined at 1050 °C (d) and Cu_2O/pearl shell composites (e).

The XRD patterns of the pearl shells and nano-Cu₂O/pearl shell composites are shown in Fig. 2. The four diffraction peaks shown in Fig. 2(1) with 2θ values of 32.30°, 37.48°, 53.94°, and 64.32° were indexed to CaO. Fig. 2(2) displays the other four diffraction peaks with 2θ values of 29.36°, 36.40°, 42.36°, and 61.34°, which were in good agreement with the characteristic peaks of crystalline Cu₂O. It can be concluded from the XRD patterns that the nano-Cu₂O/pearl shell composites obtained were composed of CaO and Cu₂O. Obviously, however, the diffraction peaks of CaO were much weaker in the composites than in the pearl shells. It was assumed that Cu₂O nanoparticles were successfully hydrolyzed on the carrier due to its alkalinity and the presence of in situ hydrolysis sites provided by the pearl shells, which changed the crystal lattice of CaO and covered the surface of the pearl shells. The average size of the Cu₂O particles calculated by the Eq. 1 was 16.8 nm. The XPS Cu 2p electron spectrum of the nano-Cu₂O/pearl shell composites, which was referenced to the binding energy of C 1s (284.6 eV), is given in Fig. 3. The two prominent binding energy peaks at 935.4 and 955.2 eV, corresponding to Cu 2$p_{3/2}$ and Cu 2$p_{1/2}$, respectively, proved the
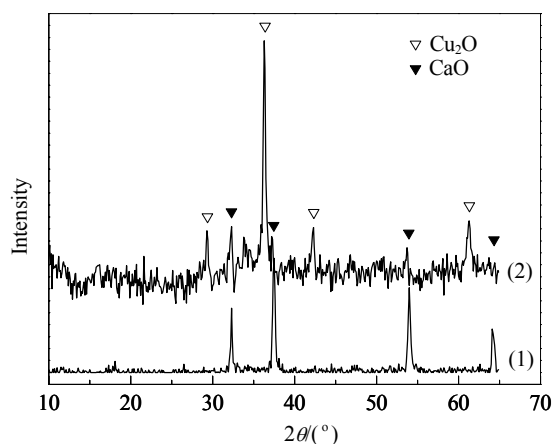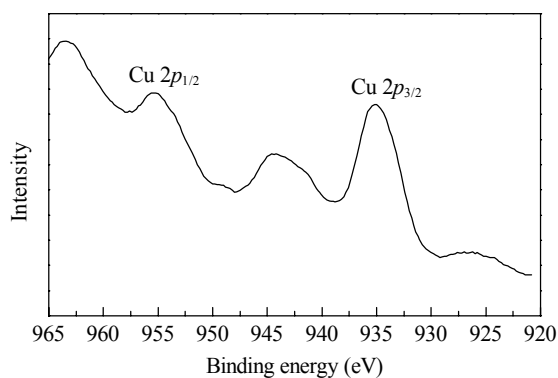
existence of the Cu(I) state [19]. The shake-up features at 944.4 and 963.6 eV demonstrated the presence of CuO on the surface of the composites [13,17], which was not observed in the XRD patterns. This indicated that the outermost surface of Cu₂O has been oxidized into a thin film of amorphous CuO, which protected and stabilized the nano-Cu₂O.

Diffuse reflectance UV-Vis spectroscopy was used to compare the optical properties of the nano-Cu₂O/pearl shell composites prepared by our method and pure nano-Cu₂O powder prepared by Hara's method [10]. As shown in Fig. 4, curve (1) exhibited a feeble spectrum for the pearl shells, especially in the visible light region from 300 to 800 nm. Both curves (2) and (3) showed a broad adsorption band from the UV to visible light ranges, indicating that both pure nano-Cu₂O and the nano-Cu₂O/pearl shell composites respond to UV and visible light. The shapes of the absorption spectra of the nano-Cu₂O/pearl shell composites and pure Cu₂O powders were similar — without red or blue shifts — which indicated that the pearl shell carrier did not affect the optical properties of the loaded Cu₂O.
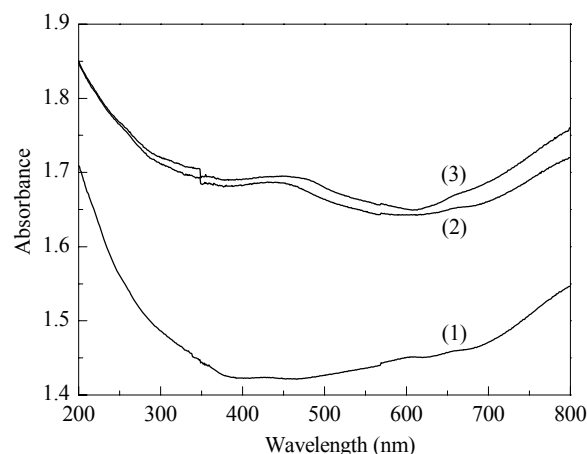
Fig. 4. Diffuse reflectance UV-Vis adsorption spectra of pearl shell carrier (1), nano-Cu₂O/pearl shell composites (2), and pure nano-Cu₂O (3).

2.2 Photocatalytic performances of the nano-Cu₂O/pearl shell composites

Figure 5 displays the photocatalytic decolorization of B-3G over the nano-Cu₂O/pearl shell composites under visible light. It is obvious that the composites were quite effective for B-3G decolorization. Due to its limited surface area because of its aggregation in aqueous solutions, pure nano-Cu₂O powders can only catalyze the degradation of 88.4% of the dyes in 30 mg/L B-3G solutions and 31.8% of the dyes in 220 mg/L B-3G solutions after 90 min irradiation. In contrast, the nano-Cu₂O/pearl shell composites degraded 98%–100% of the B-3G solutes (B-3G concentra-

Fig. 2. XRD patterns of pearl shell carriers (1) and nano-Cu₂O/pearl shell composites (2).

Fig. 3. XPS spectrum of the nano-Cu₂O/pearl shell composites.
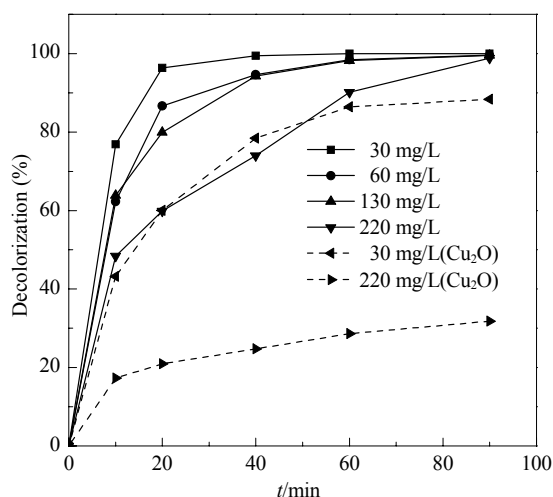
Fig. 5. Photocatalytic activity of the nano-Cu_2O/pearl shell composites as a function of the initial concentration of B-3G.

tions ≤ 220 mg/L). The highly improved photocatalytic ability of the nano-Cu_2O/pearl shell composites was due to the use of the activated pearl shell carriers. On one hand, as a highly developed adsorbent, the porous pearl shell carrier adsorbed and aggregated organic B-3G molecules to increase the contact between the catalyst Cu_2O and B-3G. Meanwhile, as the photo-electron capture agent, dissolved oxygen can easily come in contact with the well dispersed catalysts on the surface of the pearl shell carrier. Obviously, the pearl shell carrier contributed to the separation of photogenerated electrons and holes. On the other hand, the destructive adsorption on the pearl shell carrier also promoted the degradation of B-3G [20].

Figure 6 shows the photocatalytic activity of the nano-Cu_2O/pearl shell composites in different pH environments. We controlled the pH values from 6.0 to 13.0 in 60 mg/L B-3G solutions under 90 min of visible light irradiation. More than 99% of the dyes were degraded at pH ≤ 12.0. When the pH of the solution exceeded 12.0, too much
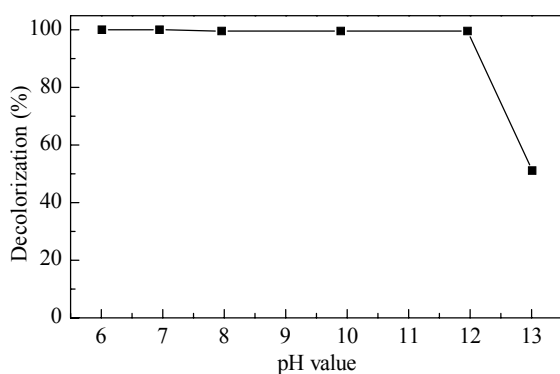
Fig. 6. Photocatalytic activity of nano-Cu_2O/pearl shell composites as a function of pH.

OH^- ions accumulated on the composite particles, which prevented electron acceptors from capturing photo-produced electrons and thereby increased the probability of electron-hole recombination. For the photocatalysis, the nano-Cu_2O/pearl shell composites were active in a broad pH range from 6.0 to 12.0.

Figure 7 shows the linear fit between ln (c_0/c) and t in the photocatalytic decolorization of B-3G over the nano-Cu_2O/pearl shell composites. Table 1 shows the corresponding first order rate constants (k), correlation coefficients (R^2), and half-life times ($t_{1/2}$). The liner relationship between ln (c_0/c) and t and the value of the correlation coefficients (R^2 ≥ 0.9780) indicated that the photocatalytic decolorization of B-3G over the nano-Cu_2O/pearl shell composites followed pseudo-first order kinetics.
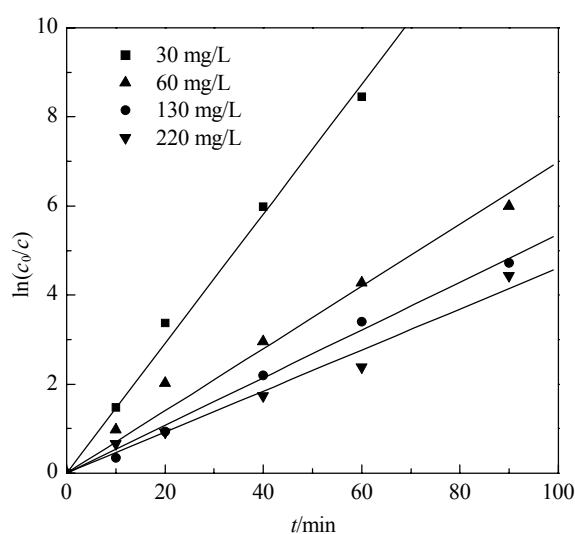
Fig. 7. Photocatalytic decolorization kinetics of B-3G at different concentrations.

Table 1 Pseudo-first order rate constants of B-3G photocatalytic decolorization at different concentrations

c_0/(mg/L)	k/min^{-1}	R^2	$t_{1/2}$/min
30	0.145	0.9947	4.78
60	0.069	0.9877	10.05
130	0.053	0.9949	13.08
220	0.046	0.9780	15.07

2.3　Formation mechanism of the Cu_2O/pearl shell composites

Figure 8(2) presents the FT-IR spectrum of the nano-Cu_2O/pearl shell composites. The peak at 3642 cm^{-1} is a characteristic peak of the pearl shell carrier, in agreement with the spectrum of CaO in the pearl shells (Fig. 8(1)). The broad peak centered at 3446 cm^{-1} corresponded to the stretching vibration of nested hydroxyl groups from adsorbed water molecules. The peak at 621 cm^{-1} corresponded

to the Cu-O vibration mode in the Cu_2O phase [21–23]. Apart from the signals of Cu_2O and CaO, the absorption peaks at 1417 and 872 cm^{-1} were due to the nano-Cu_2O/pearl shell composites, which were attributed to Ca-O-Cu bond stretching vibrations. To confirm our assignment, we calcined the nano-Cu_2O/pearl shell composites at 550 °C for 2 h. The FT-IR spectrum is shown in Fig. 8(3). After the calcination, the peaks at 3642 and 621 cm^{-1} were eliminated, but the peaks at 1417 and 872 cm^{-1} were strengthened.
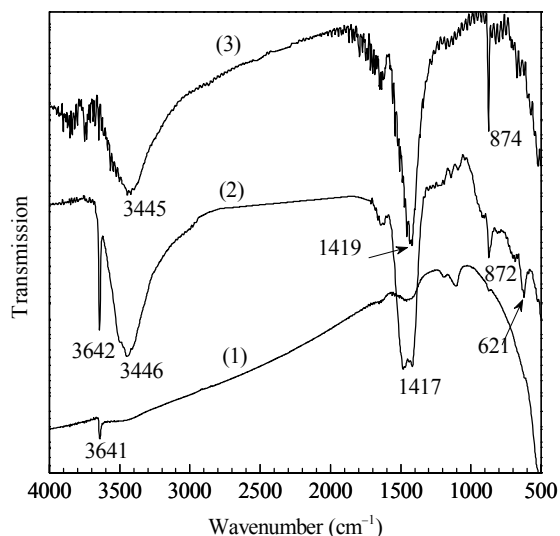
Fig. 8. FT-IR spectra of (1) pearl shell carrier, (2) nano-Cu_2O/pearl shell composites, and (3) nano-Cu_2O/pearl shell composites calcined at 550 °C for 2 h.

We suggest that there were two formation modes of the photocatalyst, which are shown in Scheme 1. First, a small part of the Cu^+ ions was hydrolyzed by dissociated OH^- ions and deposited on the surface of the pearl shells in the form of Cu_2O particles (Eq. 7). Second, most of the Cu^+ ions were first adsorbed on the pearl shells, and were then hydrolyzed in situ by OH groups on the surface of the carrier. Cu^+ ions finally combined with the pearl shell carrier in the form of $CaCu_2O_2$ (Eq. 8), which is a type of $CaCu_2O_x$ phase

Scheme 1   Schematic of the two formation modes of the photocatalyst.

[24]. Both Cu_2O and $CaCu_2O_2$ were effective catalysts for treating organic dyes.

$$2Cu^+ + 2OH^- \xrightarrow{\text{hydrolysis}} 2CuOH$$
$$\xrightarrow{\text{dehydration}} Cu_2O + H_2O \quad (7)$$
$$CaO + 2Cu^+ + 2OH^- + H_2O \xrightarrow{\text{hydrolysis}} CaCu_2(OH)_4$$
$$\xrightarrow{\text{dehydration}} CaCu_2O_2 + 2H_2O \quad (8)$$
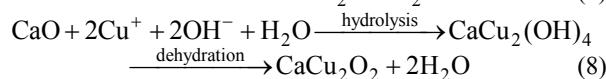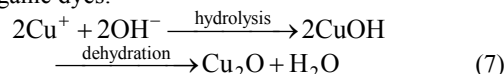
After calcination at 550 °C for 2 h, Cu_2O was oxidized to CuO (Eq. 9), and $CaCu_2O_2$ was oxidized together with CaO to $Ca_2Cu_2O_4$ (Eq. 10).

$$2Cu_2O + O_2 \xrightarrow{550\ ^oC} 4CuO \quad (9)$$
$$2CaCu_2O_2 + 2CaO + O_2 \xrightarrow{550\ ^oC} 2Ca_2Cu_2O_4 \quad (10)$$
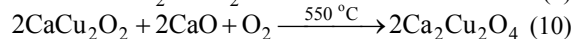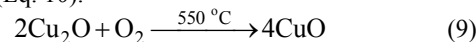
3   Conclusions

The photocatalytic decolorization of simulated wastewater containing the reactive red dye B-3G was studied. Nano-Cu_2O/pearl shell composites synthesized by in situ hydrolysis using waste pearl shells as carrier were utilized as photocatalysts under a visible light source. SEM images and XRD patterns showed the nanosize structure of the Cu_2O on these composite catalysts. The XPS spectrum showed the existence of Cu_2O and some amorphous CuO. In the UV-Vis spectra, the nano-Cu_2O/pearl shell composites had absorption bands in the UV and visible regions similar to those of pure Cu_2O. The decolorization of B-3G by the composites markedly surpassed that by pure Cu_2O, which was due to the use of the pearl shell carrier. Under our model conditions (B-3G concentration ≤ 220 mg/L, pH = 6.0–12.0, and reaction time = 90 min), the composites decolorized over 98% of the B-3G solutes. The photocatalytic reaction followed pseudo-first order kinetics. Based on the FT-IR analysis, part of the Cu^+ ions was hydrolyzed into Cu_2O deposited on the pearl shell surfaces and the other part into $CaCu_2O_2$ combined with carriers, which were all active for the photocatalytic reaction. We expect that the nano-Cu_2O/pearl shell composites can be used for the degradation of wastewater organics under natural sunlight. This work also provided waste shells a valuable use.

References

1   Yeom S H, Jung K Y. *J Ind Eng Chem*, 2009, **15**: 40

2   Nakatani N, Takamori H, Takeda K, Sakugawa H. *Bioresour Technol*, 2009, **100**: 1510

3   Yoon G L, Kim B T, Kim B O, Han S H. *Waste Manage*, 2003, **23**: 825

4   Jeon D J, Yeom S H. *Bioresour Technol*, 2009, **100**: 2646

5   Namasivayam C, Sakoda A, Suzuki M. *J Chem Technol Biotechnol*, 2005, **80**: 356

6   Hsu T C. *J Hazard Mater*, 2009, **171**: 995

7   Ji G Z, Zhu H Q, Jiang X W, Qi C Z, Zhang X M. *J Appl Polym Sci*, 2009, **114**: 3168

8 Yao N, Epstein A K, Liu W W, Sauer F, Yang N. *J Royal Soc Interface*, 2009, **6**: 367

9 Currey J D. *Proc R Soc London Ser B*, 1977, **196**: 443

10 Hara M, Kondo T, Komoda M, Ikeda S, Shinohara K, Tanaka A, Kondo J N, Domen K. *Chem Commun*, 1998: 357

11 Sun J H, Qiao L P, Sun S P, Wang G L. *J Hazard Mater*, 2008, **155**: 312

12 Kakuta S, Abe T. *Solid State Sci*, 2009, **11**: 1465

13 Zahmakiran M, Ozkar S. *Mater Lett*, 2009, **63**: 1033

14 Xu C, Wang X, Yang L C, Wu Y P. *J Solid State Chem*, 2009, **182**: 2486

15 Reddy K R, Sin B C, Yoo C H, Park W J, Ryu K S, Lee J S, Sohn D W, Lee Y I. *Scr Mater*, 2008, **58**: 1010

16 Chen J Y, Zhou P J, Li J L, Wang Y. *Carbohydr Polym*, 2008, **72**: 128

17 Yu Y, Ma L L, Huang W Y, Li J L, Wong P K, Yu J C. *J Solid State Chem*, 2005, **178**: 1488

18 Ramirez-Ortiza J, Ogura T, Medina-Valtierra J, Acosta-Ortiz S E, Bosch P, Reyes J A, de los Lara V H. *Appl Surf Sci*, 2001, **174**: 177

19 Xu Y H, Liang D H, Liu M L, Liu D Z. *Mater Res Bull*, 2008, **43**: 3474

20 Koper O, Lagadic I, Klabunde K J. *Chem Mater*, 1997, **9**: 838

21 Borgohain K, Murase N, Mahamuni S. *J Appl Phys*, 2002, **92**: 1292

22 Balamurugan B, Mehta B R, Avasthi D K, Singh F, Arora A K, Rajalakshmi M, Raghavan G, Tyagi A K, Shivaprasad S M. *J Appl Phys*, 2002, **92**: 3304

23 Xu J F, Ji W, Shen Z X, Tang S H, Ye X R, Jia D Z, Xin X Q. *J Solid State Chem*, 1999, **147**: 516

24 Deschanvres J L, Jimenez C, Rapenne L, McSporran N, Servet B, Durand O, Modreanu M. *Thin Solid Films*, 2008, **516**: 1461